Identification of XMAP215 as a microtubule-destabilizing factor in *Xenopus* egg extract by biochemical purification

Mimi Shirasu-Hiza,[1] Peg Coughlin,[2] and Tim Mitchison[2]

[1]Department of Biochemistry, University of California, San Francisco, San Francisco, CA 94114
[2]Department of Cell Biology, Harvard University Medical School, Boston, MA 02115

Microtubules (MTs) polymerized with GMPCPP, a slowly hydrolyzable GTP analogue, are stable in buffer but are rapidly depolymerized in *Xenopus* egg extracts. This depolymerization is independent of three previously identified MT destabilizers (Op18, katanin, and XKCM1/KinI). We purified the factor responsible for this novel depolymerizing activity using biochemical fractionation and a visual activity assay and identified it as XMAP215, previously identified as a prominent MT growth–promoting protein in *Xenopus* extracts. Consistent with the purification results, we find that XMAP215 is necessary for GMPCPP-MT destabilization in extracts and that recombinant full-length XMAP215 as well as an NH_2-terminal fragment have depolymerizing activity in vitro. Stimulation of depolymerization is specific for the MT plus end. These results provide evidence for a robust MT-destabilizing activity intrinsic to this microtubule-associated protein and suggest that destabilization may be part of its essential biochemical functions. We propose that the substrate in our assay, GMPCPP-stabilized MTs, serves as a model for the pause state of MT ends and that the multiple activities of XMAP215 are unified by a mechanism of antagonizing MT pauses.

Introduction

Microtubule (MT)* polymerization dynamics have been implicated in many important cellular events, including cell polarization, motility, and division. They are regulated by cellular factors that both stabilize and destabilize the MT lattice. During mitosis, for example, increased MT dynamicity allows more efficient search and capture of kinetochores by MT ends (Holy and Leibler, 1994). This increased dynamicity is driven by increases in catastrophe rate in some systems (Belmont et al., 1990) and/or decreases in rescue rate in others (Gliksman et al., 1992; Rusan et al., 2001). A number of MT dynamics regulators have been identified and characterized in recent years, and investigators in the field are actively pursuing the assignment of specific regulators to specific cellular events.

Three important MT destabilizers have been characterized in meiotic *Xenopus* egg extract: katanin (McNally and Vale,

1993), Op18/stathmin (Belmont and Mitchison, 1996), and XKCM1/MCAK (a member of the KinI family of kinesins) (Walczak et al., 1996). Of these three, the KinI family members appear to be the most important negative regulators of MT polymerization during mitosis (Belmont and Mitchison, 1996; Maney et al., 2001; Kline-Smith and Walczak, 2002). We set out to determine if there were any other MT destabilizers in *Xenopus* egg extract, using GMPCPP-stabilized MTs (CPP MTs) as the substrate in our depolymerization assays. CPP MTs were used in part for practical reasons (they are stable to dilution in buffer) and in part because they provide a novel assay that might identify factors with new mechanisms of action.

CPP MTs are stable to dilution because the nucleotide is only slowly hydrolyzed and thus mimics the GTP- or GDP-Pi–bound state (Hyman et al., 1992). However, we do not know precisely what state of physiological MTs they most closely resemble. They have been hypothesized to mimic the GTP cap, a hypothetical structure stabilizing the ends of actively growing MTs (Drechsel and Kirschner, 1994; Caplow and Shanks, 1996). In this paper, we suggest an alternative possibility, that CPP MTs most closely mimic a hypothetical "paused" state of the MT lattice, an intermediate between the growing and shrinking states (Tran et al., 1997).
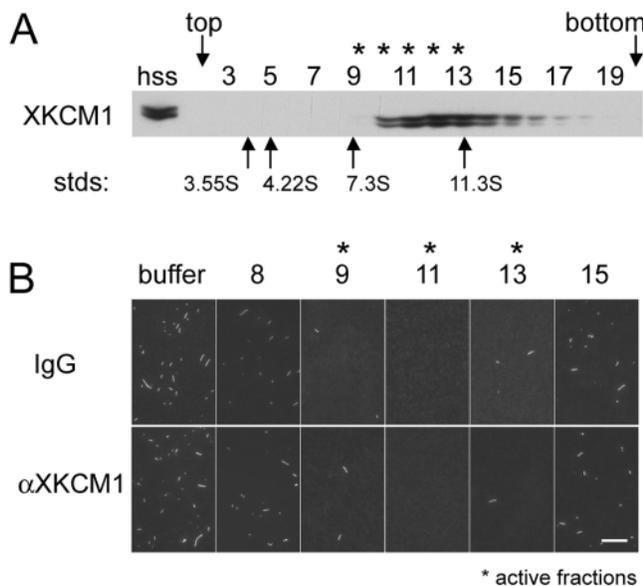
Figure 1.   **There is a CPP MT–depolymerizing activity in *Xenopus* egg extract independent of XKCM1.** (A) XKCM1 overlaps with the peak of depolymerizing activity on sucrose gradients. 50 μl of clarified CSF extract was sedimented over a 5–20% sucrose gradient. Western blot of fractions showed that XKCM1 is present in fractions 10–18. CPP MT–depolymerizing activity peaked in fractions 9–14 (see B). Arrows below the blot indicate sedimentation values for protein standards run on a parallel gradient. Active fractions are labeled with asterisks. (B) Inhibition of XKCM1 did not inhibit depolymerizing activity in sucrose gradient fractions. Fractions from the sucrose gradient shown in A were assayed for depolymerizing activity, using rhodamine-labeled CPP MTs as described in the Materials and methods. Each fraction was assayed in the absence of ATP and in the presence of random IgG or inhibitory amounts of α-XKCM1 antibody and fixed after 10 min. XKCM1 depolymerizing activity is ATP dependent. As shown, neither the absence of ATP nor the presence of αXKCM1 antibody blocked the depolymerizing activity of active fractions. Active fractions are labeled with asterisks. Bar, 10 μm.

Results

Meiotic *Xenopus* egg extracts contain a novel MT-depolymerizing factor

To assay for MT-depolymerizing factors, we added rhodamine-labeled CPP MTs to crude or clarified cytostatic factor (CSF)–arrested *Xenopus* egg extract (CSF extract) and observed their disappearance over time. CPP MTs are stable to dilution in buffer, but when added to extract, they depolymerize in 5–10 min (Caplow, M., personal communication). To characterize this depolymerizing activity, we sedimented clarified CSF extract on a 5–20% sucrose gradient and assayed fractions for depolymerizing activity. A single ATP-independent peak of activity was observed at ~9.5S (Fig. 1 B). XKCM1 cosedimented with this peak (Fig. 1 A), but katanin and Op18 did not (unpublished data). The activity appeared to be independent of XKCM1 because XKCM1 requires ATP for efficient MT depolymerization (Desai et al., 1999b). To confirm that XKCM1 was not responsible for the depolymerizing activity, we assayed those fractions in the absence of ATP and in the presence of inhibitory α-XKCM1 antibody (Walczak et al., 1996) (Fig. 1 B). Depolymerizing activity was not blocked, suggesting that another factor was responsible.

Identification of the depolymerizing activity as a fragment of XMAP215

We purified the unknown CPP MT–depolymerizing factor using conventional chromatography. The assay consisted of adding rhodamine-labeled CPP MTs to each fraction and fixing at time points to observe the disappearance of these MTs by fluorescence microscopy. Relative activity of each fraction was estimated by serial dilution. The key strategic issue was separation of the novel CPP MT–depolymerizing activity from other activities that either inhibited the assay (bundling factors) or scored in the assay (known destabilizers). To avoid confusion between the novel activity and XKCM1, we purified the novel activity from a 40% ammonium sulfate (AS) supernatant of clarified CSF extract, which contained only a fraction of total depolymerizing activity, but was free of the known depolymerizers, XKCM1, katanin, and Op18, by Western blot (unpublished data).

The CPP MT–depolymerizing factor was purified using seven steps: AS precipitation, phenyl sepharose, heparin, monoS, gel filtration, monoQ (pH 7.2), and a final monoS column. When fractions were separated by SDS-PAGE and silver stained, a set of polypeptides of ~130 kD and a protein of ~160 kD consistently coeluted with activity on the last two columns in the purification (Fig. 2, A and B, arrows). We estimated that specific activity was enriched several thousand fold by the final monoS step (Table I).

Attempts at further purification resulted in extensive loss of activity and protein. Instead, two independent purifica-

Table I. **Purification of CCP MT–depolymerizing activity from *Xenopus* egg extract**

Step	Total activity	Protein	Specific activity	Fold purification
	U	μg	U/μg	
HSS	440,000	1,320,000	0.33	1.00
AS supe	400,000	524,000	0.76	2.30
Phenyl sepharose	300,000	122,000	2.45	7.40
Heparin	150,000	2,410	62.30	188.79
MonoS 1	72,000	595	121.00	366.67
Superose 6	15,000	65	230.77	699.30
MonoQ FT	10,000	28	357.14	1,082.24
MonoS 2	4,500	5	900.00	2,727.27

Activity was defined as the maximal dilution that would depolymerize all microtubules in the visual assay within 10 min (see Materials and methods). HSS, high-speed supernatant; AS supe, 40% AS supernatant.
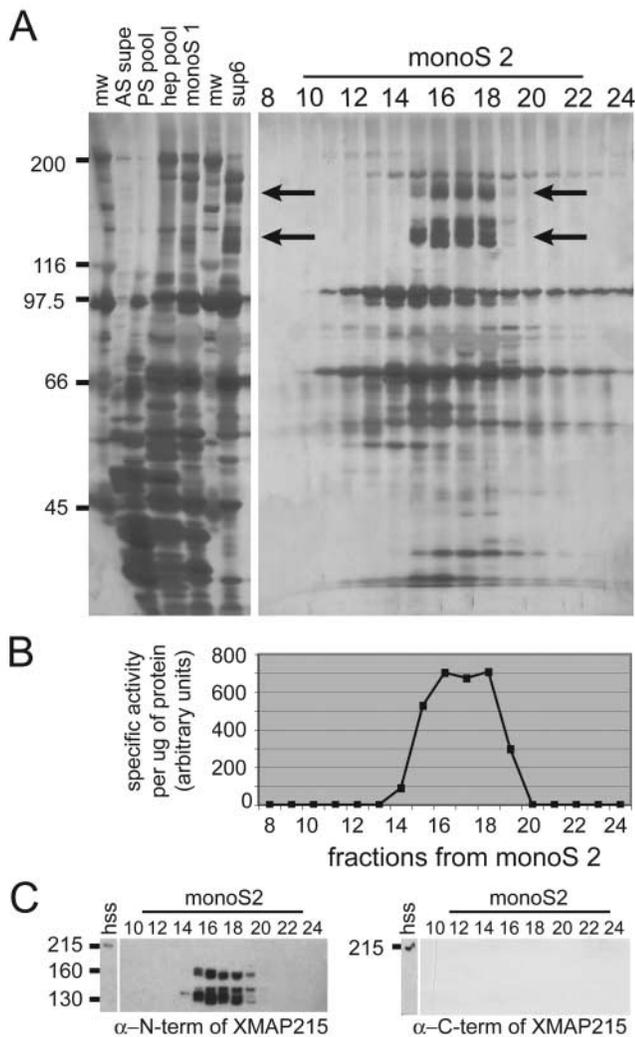
Figure 2. **Proteins of 130 and 160 kD were enriched during the purification and consistently copeaked with activity.** (A) Specific activity increased with each step of the purification, as did the prominence of p160 and p130 bands (arrows). Shown here is a silver-stained polyacrylamide gel containing fractions from the purification. Samples for the first seven lanes are listed as follows: mw, molecular weight markers; AS supe, 40% AS supernatant (5 μg protein; 4 U of specific activity); PS pool, phenyl sepharose pool of active fractions (4 μg; 10 U); hep pool, heparin pool (4.8 μg; 300 U); monoS 1, first monoS column (5 μg; 600 U); sup6, gel filtration/superose 6 (2.5 μg; 600 U). The remaining lanes (monoS2) represent fractions from the second monoS column; depolymerizing activity peaked in fractions 16, 17, and 18 (see B). Lanes loaded with these fractions each contain ∼1.3 μg of total protein and 1,260 U of specific activity. Arrows indicate p130 and p160 bands. Identity of the p130 bands (lower arrows) from these fractions was determined by mass spectrometry. (B) Activity profile for fractions for the monoS2 step. Relative activity was estimated for fractions 8–24 by serial titration in the depolymerization assay and is presented in this graph as arbitrary units per microgram protein. (C) p160 and p130 bands are NH$_2$-terminal fragments of XMAP215. Western blots of high-speed supernatant (hss) and monoS2 fractions were probed for XMAP215 with NH$_2$-terminal– or COOH-terminal–specific antibodies.

tion steps (sucrose gradient and monoQ, pH 8.8) were performed in parallel with the above purification, starting with active fractions from the gel filtration step. In both of these

steps, the same set of 130- and 160-kD proteins continued to peak in active fractions (unpublished data).

The cluster of polypeptides at 130 kD were excised from an 8% polyacrylamide gel and identified by liquid chromatography tandem mass spectrometry. 21 peptides from the tryptic digest matched the sequence of XMAP215, a previously identified 215-kD *Xenopus* MT-binding protein (Gard and Kirschner, 1987). Each of these peptides mapped to the NH$_2$-terminal half of the sequence, suggesting that we had purified an NH$_2$-terminal fragment of XMAP215 (unpublished data). Western blots using antibodies specific to the NH$_2$ and COOH termini of XMAP215 (Fig. 2 C) confirmed that the set of p130 bands as well as the p160 band enriched in our purification were NH$_2$-terminal fragments of XMAP215.

XMAP215 is a major CPP MT–depolymerizing factor in *Xenopus* egg extract

We next investigated whether XMAP215 constituted a CPP MT–depolymerizing factor in CSF extracts. Though we had purified a set of NH$_2$-terminal XMAP215 fragments from crude extract, we could not detect those fragments by Western blot in crude or clarified extract. XMAP215 appeared to exist as a full-length 215-kD species. This full-length XMAP215 comigrated with the 9.5S peak of depolymerizing activity we originally observed during sucrose gradient
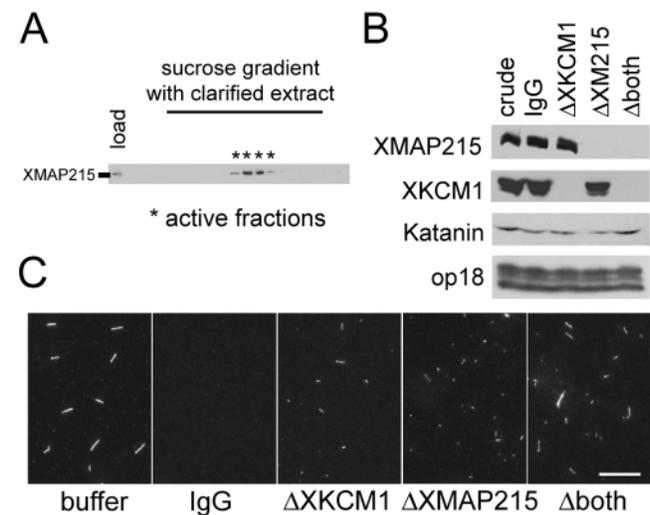
Figure 3. **XMAP215 contributes to CPP MT–depolymerizing activity in CSF extract.** (A) Full-length XMAP215 copeaks with depolymerizing activity on a sucrose gradient. Sucrose gradient fractions were analyzed by Western blot with COOH-terminal–specific α-XMAP215 antibody. Active fractions are labeled with asterisks. (B) Crude extract was specifically depleted of full-length XMAP215, XKCM1, or both. Samples were depleted with random IgG, COOH-terminal α-XMAP215 antibody (ΔXMAP215), α-XKCM1 antibody (ΔXKCM1), or both α-XMAP215 and α-XKCM1 antibodies (Δboth). Western blots for the four major depolymerizers (XMAP215, XKCM1, katanin, and Op18) are shown for each condition. (C) Depletion of XMAP215 and XKCM1 from crude extract inhibited CPP MT depolymerization. Rhodamine-labeled CPP MTs were incubated in depleted extracts for 10 min. Representative fluorescence images of each sample are shown. Buffer used for negative control was CSF-XB (extract buffer used, see Materials and methods). Bar, 10 μm.

sedimentation of clarified extract (Fig. 3 A). It is not clear if we purified a rare, truncated species of XMAP215 that is highly active in our assay or if endogenous full-length protein was proteolyzed during the purification. The latter explanation seems likely as our depolymerizing factor decreased in sedimentation value from 9.5 to 6S (unpublished data) during the purification and as XMAP215 is known to be labile to a variety of nonspecific proteases in vitro (Gard, D., personal communication).

To test if removal of this full-length XMAP215 would decrease CPP MT–destabilizing activity, crude extracts were immunodepleted of XMAP215 using a COOH-terminal antibody. Unfortunately, NH_2-terminal antibodies were not able to deplete efficiently, and NH_2-terminal fragments, if they were present, remained in the extracts. We also performed immunodepletion of XKCM1 and double depletion of both XMAP215 and XKCM1. Western blots of the depleted extracts demonstrated >95% depletion of each protein (Fig. 3 B). Levels of nondepleted protein (XKCM1 or XMAP215), as well as katanin and Op18, were unchanged in depleted extracts relative to mock-depleted extracts (Fig. 3 B). Nocodazole, a small molecule that sequesters tubulin dimer, was added to each assay to prevent endogenous tubulin from polymerizing onto the ends of the CPP MTs, as MT elongation would complicate the analysis of destabilization. Depleted extracts had spindle phenotypes similar to those previously published (Walczak et al., 1996; Tournebize et al., 2000; see Fig. S1, available at http://www.jcb.org/cgi/content/full/jcb.200211095/DC1).

When rhodamine-labeled CPP MTs were added to mock-depleted extracts, there was a large decrease in the total amount of polymer within 5 min (Fig. 3 C). In extract depleted of XMAP215, CPP MT depolymerization was partially inhibited. This inhibition was roughly similar to XKCM1 depletion and was partially restored by addition of recombinant full-length protein (unpublished data). Furthermore, depletion of both XKCM1 and XMAP215 led to less total depolymerizing activity than single depletion of either alone. In the experiment shown here, for example, at the 5-min time point, ΔXKCM1 extract had 21 times more polymer than mock-depleted extract, ΔXMAP215 had 23 times more polymer, and double-depleted extract had 37-fold more MT polymer. Evidently both proteins contribute significantly to the total CPP MT–depolymerizing activity of crude extract. MT polymer was determined by total fluorescent pixel area above background, a measurement that reflects both MT number and MT length.

XMAP215 depolymerizes CPP MTs in vitro

We next assayed pure, baculovirus-expressed XMAP215 for CPP MT–depolymerizing activity in vitro, using both full-length and truncated XMAP215 constructs previously characterized by Popov et al. (2001; see Fig. S2, available at http://www.jcb.org/cgi/content/full/jcb.200211095/DC1). Both full-length protein and an NH_2-terminal fragment (aa 1–560) were able to depolymerize rhodamine-labeled CPP MTs in vitro (Fig. 4 A). In serial titrations, activity for both polypeptides was similar and measurable, beginning between 6.25 and 12.5 nM (Fig. 4 B). The full-length protein sample does contain a small amount of cleaved protein, so we cannot definitively rule out that this is not the active species in our assay; however, the majority of the protein is full-length. The NH_2-terminal fragment does not appear to be significantly more potent than the full-length protein. A COOH-terminal fragment of XMAP215 (aa 1168–2065), on the other hand, was completely inactive in the depolymerization assay (Fig. 4, A and B). We measured depolymerizing activity in the visual assay by using fluorescent pixel area per visual field to quantitate MT polymer. Sedimentation assays and quantitation of tubulin in supernatants and pellets gave similar results (unpublished data). Samples with high concentrations of full-length XMAP215 (stoichiometric with tubulin, ~200 nM) showed less depolymerization and highly bundled MTs (Fig. 4 A). This was also seen, to a lesser ex-

Figure 4. **Pure recombinant XMAP215 depolymerizes CPP MTs in vitro.** (A) Full-length XMAP215 and an NH_2-terminal fragment of XMAP215 both depolymerize CPP MTs, but a COOH-terminal fragment does not. Rhodamine-labeled CPP MTs were incubated for 15 min in buffer containing different concentrations of full-length XMAP215 (F), an NH_2-terminal fragment (N), or a COOH-terminal fragment (C). Shown here are representative fluorescence images for four concentrations of each protein. Bar, 10 μm. (B) Full-length XMAP215 and the NH_2-terminal fragment have depolymerizing activity between 6.25 and 200 nM. MT polymer was quantitated for each sample by calculating average fluorescent pixel area per field for each protein concentration of full-length (F), NH_2-terminal (N), and COOH-terminal (C) XMAP215. MT polymer is expressed as percent median value of buffer control; error bars denote 10th and 90th percentile; the 75th, 50th, and 25th percentiles are represented by the top, middle, and bottom of each box.
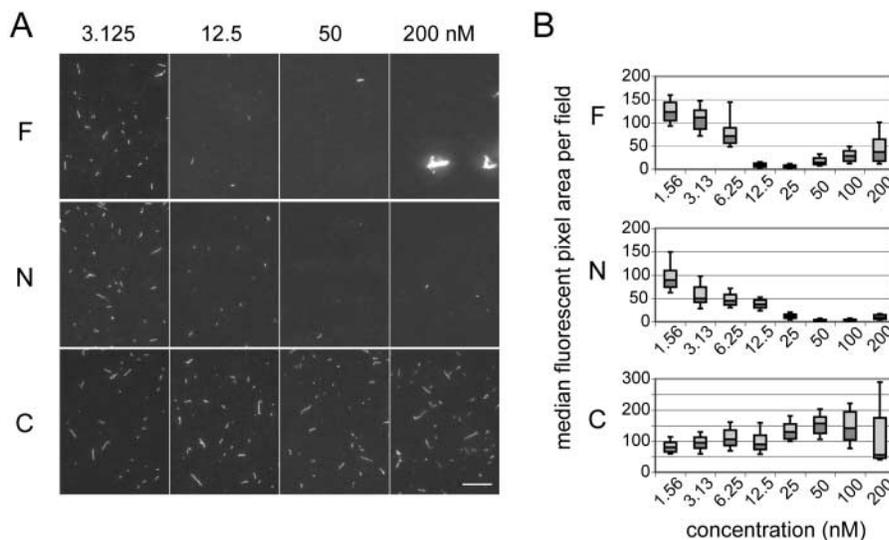
tent, in samples with very high concentrations of NH_2-terminal fragment (unpublished data). The COOH-terminal fragment did not cause bundling at any concentration.

It is not surprising that we do not normally see the polymerization-promoting activity of XMAP215 in our assay, even at concentrations similar to previously published reports. Our assay differs from dynamic MT assays in several ways that strongly select for depolymerizing activity: the assay is performed at room temperature, uses CSF-XB instead of BRB80 buffer, and contains little or no soluble tubulin dimer for polymerization. The same full-length XMAP215 construct used in our depolymerization assays was shown to have polymerization-promoting activity in dynamic MT assays (Kinoshita et al., 2001).

XMAP215-promoted depolymerization is specific to MT plus ends

To test if XMAP215 promotes CPP MT depolymerization by an end-dependent mechanism, we recorded depolymerization live in glass flow-cells using time-lapse fluorescence
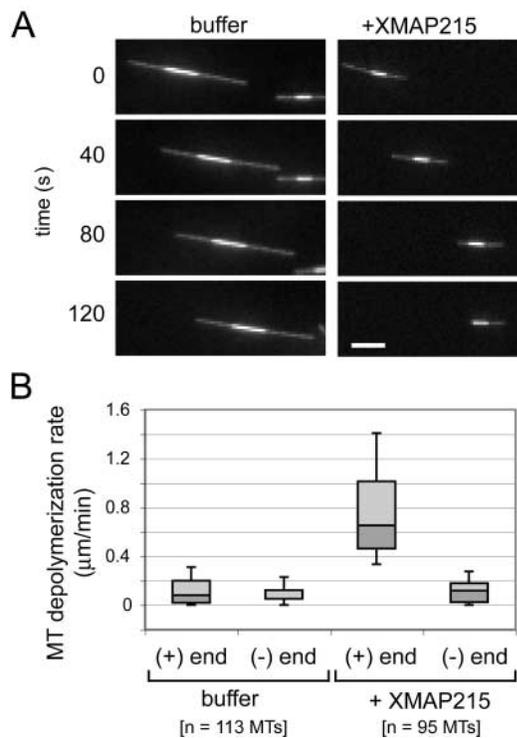
Figure 5.   **XMAP215 promotes CPP MT depolymerization at MT plus ends.** (A) XMAP215 promotes end-dependent CPP MT depolymerization. Shown here are images from a time-lapse series of dim-bright CPP MTs (see Materials and methods) treated with buffer alone or buffer plus 19 nM XMAP215 (interval between still images is 40 s). In each sample, kinesin motility was used to determine MT polarity; translocation of the MT from left to right represents minus end leading and plus end lagging. In the XMAP215-treated sample, the plus end shortens while the minus end remains stable (see Video 1, available at http://www.jcb.org/cgi/content/full/jcb.200211095/DC1). (B) Depolymerization by XMAP215 is specific to MT plus ends. Depolymerization rates were quantitated for each MT end from experiments as in A. Error bars denote 10th and 90th percentile; 75th, 50th, and 25th percentiles are represented by the top, middle, and bottom of each box.

microscopy. Rhodamine-labeled CPP MTs were bound to glass using kinesin and then treated with buffer or buffer containing XMAP215. In buffer alone, MTs were relatively stable for 30 min; in the presence of 19 nM XMAP215, they depolymerized over several minutes in an endwise fashion (Fig. 5 A). There was a strong polarity bias to depolymerization. We used dim-bright CPP MTs and kinesin motility to determine that XMAP215 depolymerized the MT plus end at a rate 5–10 times faster than buffer alone, whereas minus end depolymerization was not measurably affected (Fig. 5 B). In the presence of XMAP215, 92 out of 95 MTs (96.8%) had faster rates of depolymerization on their lagging (plus) ends than on their leading (minus) ends. Thus, XMAP215 specifically promotes CPP MT depolymerization at plus ends (see Video 1, available at http://www.jcb.org/cgi/content/full/jcb.200211095/DC1). Its polymerization-promoting activity is also plus end specific (Gard and Kirschner, 1987; Vasquez et al., 1994).

Mechanism of CPP MT depolymerization by XMAP215

There are several mechanisms by which XMAP215 might accelerate CPP MT depolymerization. XMAP215 might sequester GMPCPP-tubulin dimers, increase the rate of GMPCPP hydrolysis, or increase the dissociation rate by disrupting the lattice. We ruled out the trivial possibility that our XMAP215 protein preparation contained proteolytic activity by performing SDS-PAGE of depolymerization products (unpublished data).

To test if dimer sequestration accelerates apparent CPP MT depolymerization (by inhibiting readdition of subunits to MT ends), we added nocodazole to CPP MTs diluted in buffer alone (Fig. 6 A). The same concentration of nocodazole added before CPP MT polymerization completely inhibited polymerization (unpublished data). However, this potent monomer-sequestering drug did not stimulate depolymerization of CPP MTs in our assay, presumably because the total tubulin concentration is too low to allow significant readdition of dimer to MT ends. To test if GMPCPP was hydrolyzed during XMAP215-promoted depolymerization, we used MTs polymerized with $[\gamma\text{-}^{32}P]$GMPCPP and separated from unbound nucleotides by sedimentation through a sucrose cushion. No hydrolysis was observed in buffer or XMAP215, though Na-BRB80/60% glycerol (a positive control; Caplow et al., 1994) did stimulate hydrolysis (Fig. 6 B).

To test if XMAP215 disrupted protofilament interactions within the MT lattice, we imaged CPP MTs before and during treatment with either full-length or NH_2-terminal XMAP215 by negative-stain electron microscopy. In buffer alone, CPP MT ends were blunt (Fig. 6 C). In the presence of XMAP215 (full length or NH_2-terminal fragment), we consistently observed bulbs of material at the ends of the depolymerizing MTs. In some images, these bulbs appeared to contain curled up protofilaments. We cannot state definitively if these structures contain tubulin, XMAP215, or both; however, they are reminiscent of those resulting from treatment with KinI kinesins (Desai et al., 1999b). We favor a similar unpeeling mechanism for CPP MT depolymerization by XMAP215, though KinI and XMAP215 do differ mechanistically in two interesting
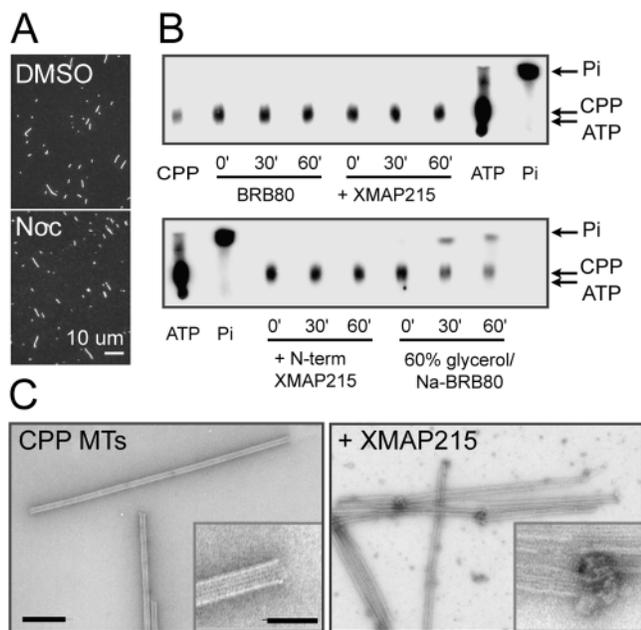
Figure 6. **Mechanism of CPP MT depolymerization by XMAP215.** (A) Nocodazole does not depolymerize CPP MTs in our assay. Dimer sequestration was tested by incubating rhodamine-labeled CPP MTs with buffer plus DMSO or 20 μM nocodazole. (B) XMAP215 does not accelerate hydrolysis of GMPCPP. TLC was used to detect the hydrolysis of γ-^{32}P–labeled GMPCPP in CPP MTs treated with buffer alone, full-length XMAP215, NH$_2$-terminal fragment of XMAP215, or Na-BRB80/60% glycerol (positive control). Time points were taken from each reaction at 0, 30, and 60 min. [γ-^{32}P]GMPCPP (CPP), [γ-^{32}P]ATP (ATP), and ^{32}Pi (Pi) are loaded as markers. Release of Pi is seen by the appearance of a second spot in Na-BRB80/60% glycerol, but not in XMAP215 or NH$_2$-terminal XMAP215 samples. Microscopy assays run in parallel demonstrated that treatment with XMAP215 and the NH$_2$-terminal construct depolymerized CPP MTs by the final time point (not depicted). (C) XMAP215 causes protofilament curling on MT ends. CPP MTs were incubated in buffer alone or buffer plus 38.5 nM full-length XMAP215 for 2 min and imaged by negative stain EM. Bars: (left) 200 nm; (right) 50 nm.

ways. First, KinI requires ATP hydrolysis to depolymerize CPP MTs efficiently, and XMAP215 does not. Second, unlike KinI, XMAP215 did not depolymerize taxol-stabilized GDP MTs (unpublished data).

Discussion

XMAP215 is a major CPP MT–depolymerizing factor in *Xenopus* egg extract

MT dynamics are subject to regulation by both stabilizing and destabilizing factors in vivo. Our overall goal in this project was to identify and characterize novel destabilizers. Although three such factors were already known in *Xenopus* egg extracts (Op18/stathmin, XKCM/KinI, and katanin), our initial experiments with CPP MTs suggested that these factors could not account for all destabilizing activity. We set out to isolate the novel factor(s) using biochemical fractionation and purified a fragment of XMAP215. We subsequently showed that XMAP215 is a major CPP MT–depolymerizing factor in *Xenopus* egg extract and that low concentrations of pure recombinant XMAP215 promote de-

polymerization of CPP MTs in vitro. XMAP215 had not previously been tested for its ability to depolymerize CPP MTs, an artificial MT substrate. We believe that this in vitro activity could have important mechanistic implications for both the molecular mechanism of XMAP215 and, more broadly, the mechanism of dynamic instability. Before discussing those mechanistic implications, we will first briefly discuss the physiological significance of our results.

Finding that XMAP215 is a major MT-destabilizing factor is at odds with the current view of this protein as an important MT growth–promoting factor. It was first discovered more than 10 yr ago by Gard and Kirschner (1987), through biochemical fractionation and a visual assay for MT polymerization, almost the converse of our depolymerization assay. Homologues exist in almost every organism, including *Saccharomyces cerevisiae* (stu2), *Schizosaccharomyces pombe* (dis1, alp14), *Caenorhabditis elegans* (zyg-9), *Drosophila melanogaster* (msps), *Arabidopsis* (mor1), and humans (ch-TOG) (for review see Ohkura et al., 2001). The two most common phenotypes for decreased levels of this protein family are short MTs and defects in spindle pole formation. In vitro, pure XMAP215 is known to promote polymerization specifically on the MT plus end (Gard and Kirschner, 1987; Vasquez et al., 1994), and careful combination of brain tubulin, XKCM1, and XMAP215 can recapitulate nearly physiological levels of all four parameters of dynamic instability (Kinoshita et al., 2001). Together, these in vivo and in vitro data have led to the model that members of the Dis1/XMAP215 family are important factors regulating physiological MT dynamics in all cells by promoting polymerization.

In light of our results, it will be interesting to investigate more closely whether Dis1/XMAP215 family members might also play a role in MT depolymerization in the cell. Consistent with this, recent work by van Breugel et al. (2003) demonstrates that the *S. cerevisiae* homologue (Stu2) does not promote MT growth in vitro but instead slows polymerization and promotes catastrophes. There are at least two places where Dis1/XMAP215 family members are candidates for site-specific depolymerizing activity. First, in fission yeast, both homologues (Dis1 and Alp14) localize to kinetochores, which are sites for plus end depolymerization (as well as polymerization) during chromosome oscillation and segregation (Garcia et al., 2001; Nakaseko et al., 2001). Tantalizingly, recent evidence in that system points to a synergistic, not antagonistic, relationship between Dis1/Alp14 and the KinI-like kinesins klp5/6 at the kinetochore (Garcia et al., 2002). Second, in every system examined to date, Dis1/XMAP215 localizes tightly to centrosomes and mitotic spindle poles (Ohkura et al., 2001). An MT-depolymerizing factor that localizes to spindle poles would be an attractive candidate for the minus end–depolymerizing activity associated with poleward MT flux. The tiny spindles that result from XMAP215 depletion in frog extract have not been tested for their flux rates. However, at least in vitro, XMAP215 depolymerization appears to be specific to MT plus ends. It is possible that XMAP215 acts as an MT polymerizer at centrosomes and an MT depolymerizer at kinetochores. Or, it is possible that XMAP215 at centrosomes depolymerizes MTs that are misoriented with their minus ends

out or, at spindle poles, depolymerizes spurious plus ends from the opposite pole. Interestingly, the major phenotype of decreasing ch-TOG levels in HeLa cells by RNAi is not MT destabilization (as would be expected for an MT stabilizer) but spindle MT disorganization (Gergely et al., 2003). Further investigation will be necessary to determine if XMAP215 ever functions in vivo as an overt depolymerizer.

Mechanistic implications for XMAP215

Although most of the literature focuses on the ability of XMAP215 to promote polymerization, our observation that XMAP215 can destabilize MTs is not without precedent. Vasquez et al. (1994) had previously shown that purified XMAP215 increased the MT depolymerization rate as well as polymerization rate, and that it inhibits rescue events. These data are consistent with lattice-destabilizing activity, as are the data of van Breugel et al. (2003) for Stu2.

Because full-length XMAP215 had depolymerizing activity in our in vitro assay, proteolysis cannot account for conversion of a polymerizing factor into a depolymerizing factor. Both polymerizing activity (Popov et al., 2001) and depolymerizing activity map roughly to the NH_2-terminal 1/4 of XMAP215. More precise mapping might separate these functions in the future. However, given that both activities act primarily on MT plus ends, our current working model is that XMAP215's polymerization-promoting and CPP MT–destabilizing activities are two aspects of a common biochemical mechanism.

What might this common mechanism be? Our preliminary studies suggest a model in which XMAP215 alters the conformation of the MT end to promote depolymerization, possibly by affecting interactions between protofilaments. The mechanism by which XMAP215 promotes polymerization specifically on the MT plus end is not known. Two hypotheses have been considered (Spittle et al., 2000): XMAP215 might oligomerize tubulin dimers in solution and thus catalyze addition of several dimers per association event; alternatively, it might alter the structure of the growing end, promoting a structure that either adds dimers more rapidly or is less likely to undergo brief pause events. The latter model, in which Dis1/XMAP215 modifies the end of the MT lattice so as to promote dynamicity, potentially allows a unified explanation for all four activities of the protein (promoting polymerization, promoting depolymerization, antagonizing/inhibiting rescue, and depolymerizing CPP MTs). A key clue might come from the specialized, nonphysiological CPP MT substrate and in understanding what physiological state it mimics most closely.

The CPP lattice has most often been used as a model for the GTP cap (Drechsel and Kirschner, 1994; Caplow and Shanks, 1996). However, the blunt-ended, closed tube structure of the CPP MT lattice is not similar to the sheet-like end of a growing MT, nor does it resemble the rams' horns of a shrinking MT (Simon and Salmon, 1990; Mandelkow et al., 1991; Chretien et al., 1995). We propose instead that CPP MTs are a model for the MT pause state. Tran et al. (1997) proposed a three-state model for dynamic instability in which the pause state is an obligate intermediate between polymerization and depolymerization. Neither the structure nor the bound nucleotide of the hypothetical pause state is

known. It seems reasonable to suggest that the pause state might have a blunt-ended, closed tube structure, intermediate between the sheet-like protofilament extensions and curled protofilaments characteristic of growth and shrinkage. Consistent with this idea, Chretien et al. (1995) proposed that loss of sheet-like protofilament extensions correlated with slower growth. A plus end that paused long enough would presumably exchange nucleotide at the exposed E-sites (Mitchison, 1993), resulting in GTP-bound tubulin subunits at the tip of a paused plus end. The exposed end of a CPP MT that is blunt and contains a GTP analogue may mimic this hypothetical blunt, exchanged state of an MT in which all the internal subunits are GDP bound.

This interpretation of what the CPP lattice mimics prompts us to propose that XMAP215 destabilizes the pause state, acting as an antipause factor (Fig. 7). MTs frequently pause in vivo, spending prolonged time neither growing nor shrinking at the resolution level of the light microscope (Shelden and Wadsworth, 1993; Tirnauer et al., 1999; Rusan et al., 2001). MTs also pause during phases of polymerization and depolymerization in *Xenopus* extracts (Tirnauer et al., 2002). Pauses are infrequent in reports of pure tubulin dynamics (Walker et al., 1988), but it is possible that pure MTs undergo micropauses too short to be detected by conventional imaging. In this pause state, MTs can theoretically transition into either growth or shrinkage, and a factor that destabilizes the pause state would increase MT dynamicity. Whether the MT transits to growth or shrinkage may depend on its environmental cues (tubulin concentration, other proteins, nucleotides, salt, or buffer); this would ex-
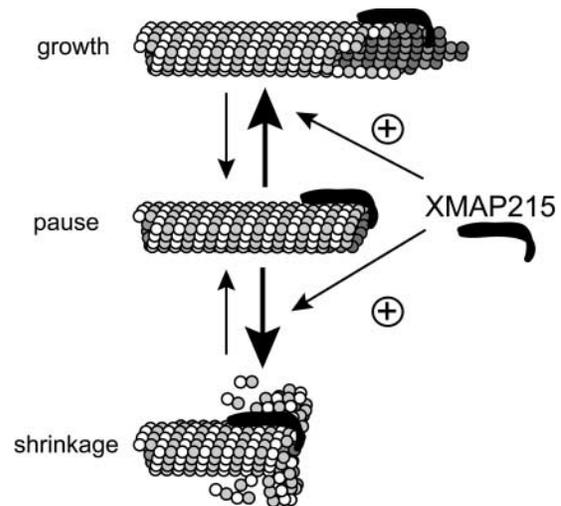
Figure 7. **Model for the potential mechanism of XMAP215 as an antipause factor.** Depicted here are the growing MT end (top) as a sheet-like structure of protofilament extensions and the shrinking MT end (bottom) with curled protofilaments (adapted from Miyamoto et al., 2002). The hypothetical paused MT end structure (middle) is positioned as an obligate intermediate between the two, drawn here with a blunt-ended, closed tube structure. We propose that XMAP215 destabilizes this pause state by weakening interprotofilament bonds and/or preventing tube closure, increasing transition to either the growing or shrinking state (arrows). Based on work by Cassimeris et al. (2001), we depict XMAP215 here as a long curved molecule that can bind protofilaments along their long axis.

plain the apparently contradictory behavior of XMAP215 in different contexts. An antipause factor would also increase both apparent polymerization and depolymerization rates if polymerization and depolymerization were rate limited by micropauses. Higher resolution tracking of growing ends with pure tubulin could test this assumption. The antipause hypothesis could also account for the plus end specificity of XMAP215 if, for example, micropauses, corresponding to loss of protofilament extensions (Chretien et al., 1995), limit plus end growth and shrinkage more than minus end growth and shrinkage. Indeed, the pause model was introduced to account for different stabilities of the plus and minus ends (Tran et al., 1997).

MT depolymerization is necessary for every aspect of mitotic spindle function, from the breakdown of MTs in prophase to the search and capture of kinetochores to kinetochore oscillations, flux, anaphase movement, and spindle disassembly after anaphase. The in vivo function of Dis1/ XMAP215, currently thought of as an MT growth–promoting factor, should be reexamined to look for functions that might depend on its MT-destabilizing activity, an equally important aspect of its biochemistry. Interesting areas of future research include determining whether the two apparently opposed activities of XMAP215 are separable, either biochemically or by mutation, and asking if XMAP215 exhibits these two activities because it is, fundamentally, an antipause factor. Addressing these questions should inform us as to the molecular mechanisms underlying physiological MT dynamics.

Materials and methods

Xenopus egg extracts

CSF-arrested extracts and in vitro spindle assembly reactions were prepared as previously described (Desai et al., 1999a). For large-scale purification, the following adjustments were made. Packing and crushing spins were performed in 50-ml (28.7 × 103.3 mm) tubes (Nalgene; Nunc), with 25–30 ml of eggs per tube. The packing spin consisted of 1 min at 500 rpm and 30 s at 1 krpm in a clinical centrifuge (Sorvall); the crushing spin was performed at 12.5 krpm (~21,000 g) for 15 min at 16°C in a Surespin 630 rotor (Sorvall). Crude CSF extract was then clarified at 4°C either in a TH-641 rotor (Sorvall) for 4 h at 41 krpm (~200,000 g) or in two AH650 rotors (Sorvall) for 2 h at 50 krpm (~235,000 g). Typically, 20–25 ml of clarified CSF extract (~40 mg/ml protein) was obtained from 1 liter of eggs (predejellying volume). Clarified extract was supplemented with cyto D (10 μg/ml final; Sigma-Aldrich), protease inhibitors (10 μg/ml final each, leupeptin, pepstatin A, chymostatin; Sigma-Aldrich), and energy mix (7.5 mM creatine phosphate, 1 mM ATP, 1 MgCl$_2$ final) before being flash frozen in liquid nitrogen in 1-ml aliquots.

In vitro assay for CPP MT depolymerization

Tubulin was labeled with tetramethyl- or X-rhodamine (Molecular Probes) as previously described (Hyman, 1991) and was used to prepare CPP MTs using standard procedures (Hyman et al., 1992; Caplow et al., 1994). Concentration of tubulin (1:3, labeled/unlabeled) during polymerization was 0.4 mg/ml (4 μM), and GMPCPP concentration was 200 μM. After polymerization at 37°C for 30 min, MTs were removed from the water bath and placed to cool at room temperature for 5–15 min. For each reaction, 0.5 μl of polymerized CPP MTs was added to 10 μl of buffer or buffer plus sample, for a final tubulin concentration of 200 nM. Reactions were staggered for fixed time points. 1 μl of each reaction was fixed with 2 μl of 80% glycerol/0.1% glutaraldehyde after 10 or 15 min incubation. During the purification, column fractions were assayed after >10-fold dilution in assay buffer (50 mM β-glycerol phosphate, pH 6.8, 50 mM sucrose, 5 mM EGTA, 1 mM DTT). When necessary, 100 μl of each fraction was desalted using 1-ml disposable spin columns filled with equilibrated G-25 fine resin. Desalting of samples with low protein concentration led to high loss of activity

unless detergent was added (0.5% CHAPS) or protein concentration supplemented to 0.5 mg/ml with purified ovalbumin (Sigma-Aldrich).

For quantitative measurement of activity with pure XMAP215 constructs, the following adjustments were made. Assays were performed in extract buffer (CSF-XB, 100 mM KCl, 50 mM sucrose, 10 mM K-Hepes, pH 7.7, 5 mM EGTA, 2 mM MgCl$_2$, 0.1 mM CaCl$_2$). After 15 min, 3 μl of each reaction was mixed thoroughly with 3 μl of fix. 2 μl of this mixture was squashed under a coverslip for a thin homogenous sample. Images (~50 random fields per sample) were acquired on an upright Nikon E-600 or E-800 microscope equipped with a cooled charge-coupled device camera (Princeton Instruments) using MetaMorph software (Universal Imaging Corp.). Images for each sample were made into a stack and thresholded using an average background value for that set (which was always much lower than the intensity of MT fluorescence). Integrated Morphometry Analysis was used to count the number of objects (MTs) per field, the length of each object, and the fluorescent pixel area of each object. Results were logged and analyzed in Microsoft Excel 2000. Average MT length can be skewed by a few long MTs in the field (versus many MTs of varied length) and average MT number per field by a large number of very small MTs. We felt that fluorescent pixel area values best represent total MT polymer as these measurements incorporate both length and number. Other parameters (such as average length × number or the average sum of MT lengths per field) would take into account both length and number but assume that all MTs are the same width; unfortunately, some fields (such as samples with high concentrations of full-length XMAP215) contained bundled MTs that were considerably wider than the average MT. Also, fluorescent pixel area was an easier parameter to quantitate for multiple fields using automated image morphology analysis. Recombinant full-length XMAP215 and truncated proteins tested in the in vitro CPP MT depolymerization assay were gifts from K. Kinoshita, D. Drechsel, and A. Hyman (Max Planck Institute, Dresden, Germany).

Determination of sedimentation value

50 μl of clarified extract or 10–20 μl of purified fraction (sup6 or monoS2) was sedimented through a 5-ml linear 5–20% sucrose gradient in assay buffer or CSF-XB (both buffers contain 50 mM sucrose on top of additional sucrose) for 5–14 h at 50 krpm in an SW50 (Beckman-Coulter) or AH650 (Sorvall) rotor. 250-μl fractions were collected from top to bottom. 20 μl of protein standard solution was run on two parallel gradients. Protein standard solution consisted of ovalbumin (3.55S), bovine serum albumin (4.3S), aldolase (7.3S), and catalase (11.3S).

Purification of XMAP215 as a CPP MT–depolymerizing factor

20 ml of *Xenopus* high-speed supernatant was thawed, pooled, and split into two 15-ml snap-cap tubes. After addition of supplemental energy mix and creatine kinase (50 μg/ml final; Sigma-Aldrich), the extract was spun in a Sorvall SA-600 rotor for 15 min at 10 krpm, 4°C. The supernatant was recovered, and 0.226 g of finely ground AS powder was added per milliliter, slowly and with continuous stirring, for a final concentration of 40% AS. Extract was rotated in the cold room for 1 h and spun for 10 min at 10 krpm in the SA-600 rotor, 4°C. Supernatant was collected and diluted fivefold into PS buffer (40% AS, 50 mM β-glycerol phosphate, 50 mM sucrose, 5 mM EGTA, 1 mM DTT). β-Glycerol phosphate served as both buffer and phosphatase inhibitor, being useful for maintaining proteins in mitotic state during purification from *Xenopus* egg extract (Takada et al., 2000). Diluted supernatant (AS supe) was syringe filtered through a 0.45-μm membrane and loaded slowly (1 ml/min) with a Gilson pump directly onto an ~30-ml XK 26/16 phenyl sepharose column (Amersham Biosciences). A 300-ml reverse gradient of 40–0% AS was applied to the column at 3 ml/min, and 10-ml fractions were collected. Activity eluted between 24 and 17% AS.

After desalting over a 50-ml HiPrep 26/10 desalting column (Amersham Biosciences) equilibrated in MS buffer (20 mM MOPS, pH 7.0, 50 mM β-glycerol phosphate, 50 mM sucrose, 5 mM EGTA, 1 mM DTT), protein (PS pool) was loaded onto a 5-ml Hi-Trap heparin column (Amersham Biosciences) and eluted with a linear 50-ml gradient up to 0.5 M KCl. Activity eluted at ~250 mM KCl. Active fractions were pooled (hep pool), supplemented with 0.5 mg/ml ovalbumin or human serum albumin final, concentrated via preblocked microcons, and rediluted until conductivity assays showed that total salt had been reduced to 0.35 mS. Pooled fractions were loaded on a 1-ml MonoS column (Amersham Biosciences) at 0.5 ml/min or, alternatively, on a 100-μl SMART system MonoS column (Amersham Biosciences) with repeated cycles of loading and elution. In both cases, >90% of the protein flowed through. Bound protein was eluted with a linear gradient of 0–500 mM KCl in MS buffer and activity eluted at 160 mM KCl.

These fractions were pooled (monoS1), concentrated via microcon to a final volume of 100 µl, refiltered through a 0.22-µm spin filter, and applied to a 1-ml SMART system Superose 6 column (Amersham Biosciences) that had been previously equilibrated with assay buffer. Activity eluted at ~1.45 ml. Four or five fractions of 50 µl each were pooled (sup6), diluted into MQ buffer (180 mM KCl, 20 mM Tris-HCl, pH 6.0, 50 mM sucrose, 5 mM EGTA, 5 mM MgCl$_2$), and loaded on a 100-µl SMART system MonoQ column (Amersham Biosciences). Activity appeared in the flowthrough (Q FT), which was supplemented with MOPS to pH 7.0 and diluted to a final KCl concentration of 50 mM. The Q FT was applied to a 100-µl SMART system MonoS column (Amersham Biosciences). During a linear gradient of 0–500 mM KCl, a single peak of activity again eluted at 160 mM KCl. 50-µl fractions (monoS2) were collected and assayed. Fractions were pooled and sedimented on a 2-ml 5–20% sucrose gradient (TLS-55 rotor, 50 krpm, 4 h, 4°C) or run on SDS-PAGE for silver stain.

Purification was complicated by nonspecific losses in activity when protein concentration was too low. For this reason, in the last two or three steps, protein levels were supplemented to 0.5 mg/ml during column loading with purified ovalbumin, which binds monoQ and flows through monoS in our MQ and MS buffers, respectively. As losses in activity were also incurred by freeze–thaw, the purification protocol was performed over several days at 4°C, without freezing any active fractions.

Mass spectrometry
MonoS final fractions were separated on an 8% polyacrylamide gel by SDS-PAGE. The gel was silver stained with the following protocol: 10 min in 50% methanol; 10 min in 5% methanol; 10 min in 250 ml H$_2$O containing 8 µl of 1 M DTT; 10 min in silver solution (0.2% AgNO$_3$); brief wash with milliQ water (3 × 10 s); brief wash with a small amount of developing solution (7.5 g of Na$_2$CO$_3$ in 250 ml water plus 125 µl 37% formaldehyde); brief wash with a small amount of milliQ water; addition of the remaining developing solution until bands are of desired intensity; quench by pouring off developing solution and adding 5% AcOH; 3 × 15 min washes with water. After silver stain, p130 bands were carefully excised and subjected to tryptic digest before liquid chromatography tandem mass spectrometry and database analysis; these procedures were performed at Taplin Biological Mass Spectrometry Facility at Harvard Medical School.

Immmunoreagents
Antibodies specific to the NH$_2$-terminal 560 aa of ch-TOG and antibodies specific to the COOH-terminal 15 aa of ch-TOG were a gift from K. Kinoshita and A. Hyman. Anti-katanin antibody was a gift from F. McNally (University of California, Davis, CA). Inhibitory XKCM1 antibodies were provided by both C. Walczak (University of Indiana, Bloomington, IN) and R. Ohi (Harvard University) inhibitory activity was confirmed both in extract (Fig. 3 D) and in in vitro assays with recombinant XKCM1 (not depicted). Immunodepletion of *Xenopus* egg extracts was performed with Dynabeads as previously described (Tournebize et al., 2000). Efficient depletion of XMAP215 was achieved using a polyclonal rabbit antibody raised against the last 16 aa at the COOH terminus after two rounds of depletion, using 12.5 µg of antibody per 50 µl of beads per round for 140 µl of crude extract. Similar concentrations of rabbit IgG (Sigma-Aldrich) and anti-XKCM1 antibody were used for each round of mock and XKCM1 depletions.

Time-lapse microscopy and flow cell assay
Flow cells were constructed using GoldSeal glass slides, 18 × 18-mm square GoldSeal coverslips, and thin strips of double-sided Scotch tape. Each coverslip was rinsed in acetone for 10–15 min before being spun dry and then air dried on Whatman paper (15–30 min). Coverslips were inverted onto two pieces of double-sided tape stuck to a glass slide, creating chambers of ~10–15 µl. Reagents were pipetted into one end and drawn out the other with triangles of whatman paper in this order: (1) 1 vol of 100 µg/ml kinesin (gift from Z. Maliga, Harvard University) in 20 mM Tris-HCl, pH 7.0, 1 mM DTT, incubated 10 min; (2) 5–8 vol of 6.5 mg/ml casein, incubated 10 min; (3) 5–8 vol BRB80 + 1 mM DTT; (4) 3–5 vol of CPP MTs, usually diluted to 400 nM, incubated 10 min; (5) 5–8 vol BRB80 + 1× oxygen scavenging mix (OS, 4.5 mg/ml glucose, 0.035 mg/ml catalase, 0.2 mg/ml glucose oxidase, 0.5% β-mercaptoethanol in CSF-XB); (6) 5–8 vol CSF-XB + OS; (7) 3–5 vol CSF-XB + OS ± 19 nM XMAP215 (full-length recombinant protein) ± 10 µM MgATP. Though kinesin motility was fast and reliable in BRB80, CPP MTs were often released by kinesin in CSF-XB + ATP, necessitating high concentrations of kinesin in step 1 and low ATP concentrations in step 7. Dim-bright CPP MTs were made as previously described (Hyman, 1991), polymerizing 0.4 mg/ml of 1:1 (labeled/unlabeled) tubulin plus 200 µM CPP for bright seeds and using 36 µg/ml of these seeds in ~0.2 mg/ml of 1:7 (labeled/unlabeled) tubulin for dim MT

elongation. Time-lapse movies were made by taking 100-ms exposures (bin = 2) every 5–15 s, using microscopy equipment as described above. Movies were analyzed using Metamorph as follows: movies were recorded as stacks; planes corresponding to two time points were duplicated from the stack; using color combine, the two planes were overlaid in two different colors; using the line region tool, MT lengths were measured on either side of a fiducial mark; polarity could be assigned by comparing the location of the fiducial mark in each plane. We only used MTs with clearly distinguishable ends in both planes and clear movement of the fiducial mark. MT length measurements were logged to a spreadsheet in Microsoft Excel for further analysis.

GMPCPP hydrolysis
[γ-^{32}P]GMPCPP was synthesized from GMPCP and [γ-^{32}P]ATP. 2 U of nucleotide diphosphate kinase (Sigma-Aldrich), 15 µl of 1 mM GMPCP in BRB80, and 15 µl of [γ-^{32}P]ATP were incubated at room temperature for 6 h. The reaction was spun for 15 min in a microfuge, and the supernatant was filtered through a 10K cut-off filter. 0.1 µl of each reaction product was analyzed by TLC using PEI-cellulose plates (Baker-Flex) run in 1.0 M LiCl and detected using a phosphorimager (Molecular Imager FX; Bio-Rad Laboratories) and Quantity One v.4.1.1 software. Standards (1 µl each of 10 mM GMPCPP, ATP stocks) were run in parallel and detected using a handheld UV lamp.

[γ-^{32}P]GMPCPP was used to monitor phosphate hydrolysis in the depolymerization reaction. Depolymerization reactions were performed as described above, using 75 nM full-length, recombinant XMAP215 or NH$_2$-terminal fragment, except that 15 µl of [γ-^{32}P]GMPCPP was added during CPP MT polymerization to incorporate it into the lattice. Reactions without [γ-^{32}P]GMPCPP were performed in parallel, to monitor the extent of depolymerization by visual assay. Phosphate hydrolysis was monitored by taking 6.7 µl of each reaction at 0, 10, and 20 min for assays in assay buffer and at 0, 30, and 60 min for assays performed in BRB80 or BRB80 + 5 mM EDTA. Results were equivalent for each buffer condition. Time points were quenched by addition of an equal volume of denaturing buffer (8 M urea, 20 mM Tris-HCl, pH 7.0, 5 mM EDTA). As a positive control, depolymerization reactions were performed in 60% glycerol/Na-BRB80, which is known to induce hydrolysis of GMPCPP. Free ^{32}Pi was separated from [γ-^{32}P]GMPCPP by TLC on PEI-cellulose using 0.75 M sodium phosphate, pH 4.2, after first prerunning (postload) each TLC plate with ddH$_2$O to get rid of excess salt, urea, and glycerol. Radioactive reaction products were detected using a Molecular Imager FX phosphorimager and Quantity One v.4.1.1 software.

Negative stain EM
Negative stain EM was performed as previously described (Desai et al., 1999b). Standard depolymerization reactions were performed, using 38.5 nM XMAP215, except that each sample was spun for 15 min on high at 4°C in a microfuge before addition of rhodamine-labeled CPP MTs, and reactions were performed in BRB80 buffer.

Online supplemental material
The supplemental material (Figs. S1 and S2; Video 1) is available at http://www.jcb.org/cgi/content/full/jcb.200211095/DC1. Fig. S1 shows representative fluorescent images of spindles made in extracts depleted with control (IgG), αXKCM1, or αXMAP215 antibodies. Fig. S2 is a Coomassie-stained gel of the three XMAP215 constructs used in in vitro depolymerization assays. Video 1 is a time-lapse video of dim-bright microtubules treated first with buffer alone and then with buffer plus 19 µM XMAP215. The microtubules are being translocated with their minus ends leading.

References

Belmont, L.D., and T.J. Mitchison. 1996. Identification of a protein that interacts with tubulin dimers and increases the catastrophe rate of microtubules. *Cell.* 84:623–631.

Belmont, L.D., A.A. Hyman, K.E. Sawin, and T.J. Mitchison. 1990. Real-time visualization of cell cycle-dependent changes in microtubule dynamics in cytoplasmic extracts. *Cell.* 62:579–589.

Caplow, M., and J. Shanks. 1996. Evidence that a single monolayer tubulin-GTP cap is both necessary and sufficient to stabilize microtubules. *Mol. Biol. Cell.* 7:663–675.

Caplow, M., R.L. Ruhlen, and J. Shanks. 1994. The free energy for hydrolysis of a microtubule-bound nucleotide triphosphate is near zero: all of the free energy for hydrolysis is stored in the microtubule lattice. *J. Cell Biol.* 127:779–788.

Cassimeris, L., D. Gard, P.T. Tran, and H.P. Erickson. 2001. XMAP215 is a long thin molecule that does not increase microtubule stiffness. *J. Cell Sci.* 114:3025–3033.

Chretien, D., S.D. Fuller, and E. Karsenti. 1995. Structure of growing microtubule ends: two-dimensional sheets close into tubes at variable rates. *J. Cell Biol.* 129:1311–1328.

Desai, A., A. Murray, T.J. Mitchison, and C.E. Walczak. 1999a. The use of *Xenopus* egg extracts to study mitotic spindle assembly and function in vitro. *Methods Cell Biol.* 61:385–412.

Desai, A., S. Verma, T.J. Mitchison, and C.E. Walczak. 1999b. Kin I kinesins are microtubule-destabilizing enzymes. *Cell.* 96:69–78.

Drechsel, D.N., and M.W. Kirschner. 1994. The minimum GTP cap required to stabilize microtubules. *Curr. Biol.* 4:1053–1061.

Garcia, M.A., L. Vardy, N. Koonrugsa, and T. Toda. 2001. Fission yeast ch-TOG/XMAP215 homologue Alp14 connects mitotic spindles with the kinetochore and is a component of the Mad2-dependent spindle checkpoint. *EMBO J.* 20:3389–3401.

Garcia, M.A., N. Koonrugsa, and T. Toda. 2002. Spindle-kinetochore attachment requires the combined action of Kin I-like Klp5/6 and Alp14/Dis1-MAPs in fission yeast. *EMBO J.* 21:6015–6024.

Gard, D.L., and M.W. Kirschner. 1987. A microtubule-associated protein from *Xenopus* eggs that specifically promotes assembly at the plus end. *J. Cell Biol.* 105:2203–2215.

Gergely, F., V.M. Draviam, and J.W. Raff. 2003. The ch-TOG/XMAP215 protein is essential for spindle pole organization in human somatic cells. *Genes Dev.* 17:336–341.

Gliksman, N.R., S.F. Parsons, and E.D. Salmon. 1992. Okadaic acid induces interphase to mitotic-like microtubule dynamic instability by inactivating rescue. *J. Cell Biol.* 119:1271–1276.

Holy, T.E., and S. Leibler. 1994. Dynamic instability of microtubules as an efficient way to search in space. *Proc. Natl. Acad. Sci. USA.* 91:5682–5685.

Hyman, A.A. 1991. Preparation of marked microtubules for the assay of the polarity of microtubule-based motors by fluorescence. *J. Cell Sci. Suppl.* 14:125–127.

Hyman, A.A., S. Salser, D.N. Drechsel, N. Unwin, and T.J. Mitchison. 1992. Role of GTP hydrolysis in microtubule dynamics: information from a slowly hydrolyzable analogue, GMPCPP. *Mol. Biol. Cell.* 3:1155–1167.

Kinoshita, K., I. Arnal, A. Desai, D.N. Drechsel, and A.A. Hyman. 2001. Reconstitution of physiological microtubule dynamics using purified components. *Science.* 294:1340–1343.

Kline-Smith, S.L., and C.E. Walczak. 2002. The microtubule-destabilizing kinesin XKCM1 regulates microtubule dynamic instability in Cells. *Mol. Biol. Cell.* 13:2718–2731.

Mandelkow, E.M., E. Mandelkow, and R.A. Milligan. 1991. Microtubule dynamics and microtubule caps: a time-resolved cryo-electron microscopy study. *J. Cell Biol.* 114:977–991.

Maney, T., M. Wagenbach, and L. Wordeman. 2001. Molecular dissection of the microtubule depolymerizing activity of mitotic centromere-associated kinesin. *J. Biol. Chem.* 276:34753–34758.

McNally, F.J., and R.D. Vale. 1993. Identification of katanin, an ATPase that severs and disassembles stable microtubules. *Cell.* 75:419–429.

Mitchison, T.J. 1993. Localization of an exchangeable GTP binding site at the plus end of microtubules. *Science.* 261:1044–1047.

Miyamoto, D., Z. Perlman, T. Mitchison, and M. Shirasu-Hiza. 2002. Dynamics of the mitotic spindle - potential therapeutic targets. *In* Progress in Cell Cycle Research. Vol. 5. L. Meijer, A. Jezequel, and M. Roberge, editors. Plenum Press, New York. 349–360.

Nakaseko, Y., G. Goshima, J. Morishita, and M. Yanagida. 2001. M phase-specific kinetochore proteins in fission yeast: microtubule-associating Dis1 and Mtc1 display rapid separation and segregation during anaphase. *Curr. Biol.* 11:537–549.

Ohkura, H., M.A. Garcia, and T. Toda. 2001. Dis1/TOG universal microtubule adaptors - one MAP for all? *J. Cell Sci.* 114:3805–3812.

Popov, A.V., A. Pozniakovsky, I. Arnal, C. Antony, A.J. Ashford, K. Kinoshita, R. Tournebize, A.A. Hyman, and E. Karsenti. 2001. XMAP215 regulates microtubule dynamics through two distinct domains. *EMBO J.* 20:397–410.

Rusan, N.M., C.J. Fagerstrom, A.M. Yvon, and P. Wadsworth. 2001. Cell cycle-dependent changes in microtubule dynamics in living cells expressing green fluorescent protein-α tubulin. *Mol. Biol. Cell.* 12:971–980.

Shelden, E., and P. Wadsworth. 1993. Observation and quantification of individual microtubule behavior in vivo: microtubule dynamics are cell type specific. *J. Cell Biol.* 120:935–945.

Simon, J.R., and E.D. Salmon. 1990. The structure of microtubule ends during the elongation and shortening phases of dynamic instability examined by negative-stain electron microscopy. *J. Cell Sci.* 96(Pt 4):571–582.

Spittle, C., S. Charrasse, C. Larroque, and L. Cassimeris. 2000. The interaction of TOGp with microtubules and tubulin. *J. Biol. Chem.* 275:20748–20753.

Takada, S., T. Shibata, Y. Hiraoka, and H. Masuda. 2000. Identification of ribonucleotide reductase protein R1 as an activator of microtubule nucleation in *Xenopus* egg mitotic extracts. *Mol. Biol. Cell.* 11:4173–4187.

Tirnauer, J.S., S. Grego, E.D. Salmon, and T.J. Mitchison. 2002. EB1-microtubule interactions in *Xenopus* egg extracts: role of EB1 in microtubule stabilization and mechanisms of targeting to microtubules. *Mol. Biol. Cell.* 13:3614–3626.

Tirnauer, J.S., E. O'Toole, L. Berrueta, B.E. Bierer, and D. Pellman. 1999. Yeast Bim1p promotes the G1-specific dynamics of microtubules. *J. Cell Biol.* 145:993–1007.

Tournebize, R., A. Popov, K. Kinoshita, A.J. Ashford, S. Rybina, A. Pozniakovsky, T.U. Mayer, C.E. Walczak, E. Karsenti, and A.A. Hyman. 2000. Control of microtubule dynamics by the antagonistic activities of XMAP215 and XKCM1 in *Xenopus* egg extracts. *Nat. Cell Biol.* 2:13–19.

Tran, P.T., R.A. Walker, and E.D. Salmon. 1997. A metastable intermediate state of microtubule dynamic instability that differs significantly between plus and minus ends. *J. Cell Biol.* 138:105–117.

van Breugel, M., D. Drechsel, and A. Hyman. 2003. Stu2p, the budding yeast member of the conserved Dis1/XMAP215 family of microtubule-associated proteins is a plus end–binding microtubule destabilizer. *J. Cell Biol.* 161:359–369.

Vasquez, R.J., D.L. Gard, and L. Cassimeris. 1994. XMAP from *Xenopus* eggs promotes rapid plus end assembly of microtubules and rapid microtubule polymer turnover. *J. Cell Biol.* 127:985–993.

Walczak, C.E., T.J. Mitchison, and A. Desai. 1996. XKCM1: a *Xenopus* kinesin-related protein that regulates microtubule dynamics during mitotic spindle assembly. *Cell.* 84:37–47.

Walker, R.A., E.T. O'Brien, N.K. Pryer, M.F. Soboeiro, W.A. Voter, H.P. Erickson, and E.D. Salmon. 1988. Dynamic instability of individual microtubules analyzed by video light microscopy: rate constants and transition frequencies. *J. Cell Biol.* 107:1437–1448.